Heterodyne Detection of Low-Frequency Fields via Rydberg EIT with Phase Demodulation

Shenchao Jin[1,2†], Xiayang Fan[1,2†], Xin Wang[1,2], Yi Song[1,2], and Yuan Sun[1,2*]

[1]*Shanghai Institute of Optics and Fine Mechanics, Chinese Academy of Sciences, Shanghai 201800, China*
[2]*University of Chinese Academy of Sciences, Beijing 100049, China*

(Received 10 September 2025; accepted manuscript online 9 October 2025)

Recently, the rapid progress of quantum sensing research reveals that Rydberg atoms have great potential in becoming high-precision centimeter-scale antennas for low-frequency fields. In order to facilitate efficient and reliable detection of low-frequency fields via Rydberg atoms, we designed and implemented a heterodyne method based on the linear response to external signals under the condition of Rydberg electromagnetically induced transparency (EIT). Instead of relying on observing changes in the absorption of light by Rydberg atoms, our method focuses on the phase modulation effect on the probe laser induced by low-frequency fields via the Rydberg EIT mechanism and utilizes a special demodulation process to accurately retrieve signals including both amplitude and phase. The general principles of our method apply to both electric and magnetic fields, and it is even possible to realize a combination of both functionalities in the same apparatus. In particular, we experimentally demonstrate the full cycle of operations with respect to both cases. In measuring low-frequency electric fields, we discover that the Rydberg dipole–dipole interaction among atoms induces a linear superposition of Rydberg states with different angular momentum, generating a first-order response corresponding to the signature of the linear Stark effect. As Rydberg atoms have excellent coupling strengths with electric fields, our results indicate that our method can hopefully achieve high-precision performance for practical tasks in the future.

DOI: 10.1088/0256-307X/42/11/110304 CSTR: 32039.14.0256-307X.42.11.110304

In recent years, Rydberg atoms have been making solid progress in quantum sensing[1–3] and quantum computation.[4] The key advantage of natural or artificial atoms' Rydberg states is their much greater coupling strength with electric fields compared to ground states, yielding significant potential for high-precision, compact quantum sensors of electric signals. Quantum sensing of microwave[5–13] and THz[14] electric fields via Rydberg atoms has already become a standard routine in various applications,[15,16] and the pursuit of higher-level optoelectric integration has begun.[17–20] Recently, it has been discovered that Rydberg atoms have the potential to serve as excellent candidates for centimeter-scale antennas for low-frequency fields when equipped with advanced quantum coherent control methods,[21] which relies on the amplitude or phase modulation effects on the probe light induced by the external fields.[22] Further development faces several major obstacles including the shielding effect from alkali atoms coating the vapor cell walls and scalability challenges in building larger systems to achieve theoretically predicted high sensitivity.[23] At this moment, many investigations in this direction rely on built-in electrodes within the vapor cell to induce interaction between low-frequency electric fields and Rydberg atoms.[24,25]

On the other hand, quantum sensing of low-frequency and radio-frequency magnetic fields by optical magnetometry with alkali atom vapor has achieved impressive performance.[26,27] A prominent example[28] is the optically pumped magnetometer,[29–32] achieving sub-fT sensitivity in the spin-exchange relaxation-free regime.[33,34] Alternatively, atomic magnetometers based on nonlinear magneto-optical rotation,[35] which share physical principles with coherent population trapping (CPT)[36] and typically operate below 100 Hz[37,38] due to CPT's narrow linewidth, can extend the effective detection range to kHz region at the expense of sensitivity.

Aiming for a systematic, low-cost, and scalable solution for high-sensitivity detection of low-frequency electric fields with reasonable frequency response properties, we propose, analyze, and experimentally demonstrate a special demodulation method with heterodyne processes to fully resolve the signal in the sense of all-optical detection under the condition of Rydberg electromagnetically induced transparency (EIT).

We explain the basic principles via a typical three-level system with two-photon ground-Rydberg transition as shown in Fig. 1(b). The probe laser always stays resonant with the transition $|g\rangle \leftrightarrow |e\rangle$ while the coupling laser of Rabi frequency Ω_c stays resonant with the transition $|e\rangle \leftrightarrow |r\rangle$. When the external field perturbs the Rydberg state $|r\rangle$, the coupling laser will subsequently experience a non-vanishing two-photon detuning Δ. We can define α_0

†These authors contributed equally to this work.
*Corresponding author. Email: yuansun@siom.ac.cn
© 2025 Chinese Physical Society and IOP Publishing Ltd. All rights, including for text and data mining, AI training, and similar technologies, are reserved.

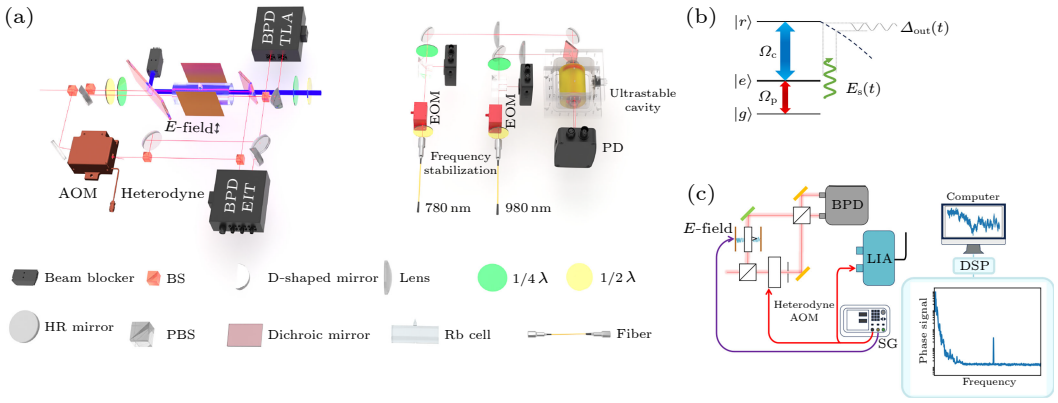

Fig. 1. (a) Schematics of the experimental setup. More details are provided in the Supplementary Materials (SM). (b) Level diagram of idealized three-level two-photon ground-Rydberg transition. (c) Heterodyne, detection, and post-processing parts of experimental apparatus, showing the basics of demodulation processes. AOM: acousto-optic modulator; SG: signal generator; PD: photodiode; BPD: balanced photodiode; LIA: lock-in amplifier; DSP: digital signal processor.

as unsaturated resonant absorption coefficient $\alpha_0 = \frac{2\pi\nu_p N\mu_{ge}^2}{2\hbar c\epsilon_0\gamma_e}$ with ν_p as the probe laser frequency, N as the atom number density, μ_{ge} as the atomic dipole moment of transition $|g\rangle \leftrightarrow |e\rangle$ and γ_e as the decay rate of $|e\rangle$. The linear susceptibility χ contains the real part $\Re\chi$ and imaginary part $\Im\chi$.[36,39,40] Here $\Re\chi(\Delta)$ generates an effective phase change on the probe laser,

$$\Re\chi(\Delta) = \frac{c\Delta|\Omega_c|^2\alpha_0}{\pi\nu_p\gamma_e(\gamma_{\text{eff}}^2+\Delta^2)}, \quad \text{with } \gamma_{\text{eff}} = \gamma_r + \frac{|\Omega_c|^2}{\gamma_e}, \quad (1)$$

where γ_r is the decay rate of $|r\rangle$.

We prefer that the experiment operates under the strong coupling regime $|\Omega_c|^2 \gg \gamma_e\gamma_r$ to yield a good transparency condition. Meanwhile, the performance of phase detection works well under the condition that the frequency variation range of the incoming signal stays within the transparency window of Rydberg EIT, which suits low-frequency fields. The magnetic field perturbs the Rydberg state via the Zeeman effect while the electric field perturbs it via the Stark effect. Consequently, the low-frequency field drives Δ, as in Eq. (1), into a time-dependent term. An incoming signal of frequency ω_l induces a phase modulation $\beta_l\cos(\omega_l t+\phi_l)$ in the probe laser to the first order, where β_l describes the strength of modulation and ϕ_l represents the initial phase. According to Eq. (1), when $|\Delta|$ is relatively small, the first-order effect is given by

$$\Re\chi(\Delta) = \frac{c|\Omega_c|^2\alpha_0}{\pi\nu_p\gamma_e\gamma_{\text{eff}}^2}\Delta + \mathcal{O}(|\Delta|^3). \quad (2)$$

Figure 1(a) outlines the experimental setup. We choose an enriched ^{87}Rb vapor cell at room temperature, and the optical depth is about 0.2. The coherent ground-Rydberg excitation, as well as the phase modulation and demodulation in the experiment, all stem from a 480 nm laser and a 780 nm laser. The 780 nm laser couples the ground state $|g\rangle$ of $5^2S_{1/2}$, $F = 2$, to the excited state $|e\rangle$ of $5^2P_{3/2}$, $F = 3$, with a beam waist of 0.3 mm. The 480 nm laser couples the excited state $|e\rangle$ to the Rydberg state $|r\rangle$, with a beam waist of 0.4 mm. In the magnetic field measurement, the vapor cell is cylindrical in shape with a diameter of 25 mm and a length of 100 mm. In the electric field measurement, the vapor cell is cuboidal in shape with dimensions of 25 mm × 25 mm × 50 mm.

The 780 nm laser is first split into the reference and probe beams, and then we divide the 780 nm probe beam into EIT probe and two-level-atom (TLA) probe beams. The 480 nm laser counter-propagates with the EIT probe laser, and both lasers are locked to one ultra-low expansion high-finesse cavity made by Qingyuan Tianzhiheng Quantum Technology. In the heterodyne section, the 780 nm reference laser undergoes a 50 MHz frequency shift ω_h and subsequently mixes with the EIT probe laser. Then the beat signal contains information about both the carrier ω_h and the incoming low-frequency signal $\cos[\omega_h t+\beta_l\cos(\omega_l t+\phi_l)]$. Through two layers of demodulation efforts or lock-in amplification, information about the incoming low-frequency field can be recovered. In the first layer, from the beat signal oscillating around ω_h, a lock-in amplifier extracts the effective low-frequency modulation component $\beta_l\cos(\omega_l t+\phi_l)$ without compromising amplitude or phase information. The second layer focuses on the low-frequency range of interest, which generates eventual output data via a second lock-in amplifier, spectrum analyzer, or digital signal processor with similar purposes. In comparison, here the heterodyne method avoids locking interferometer troubles,[41] while bearing more robustness in practical implementation.

Applying a dc bias field with Rydberg atoms has been common practice in measuring dc electric fields[42,43] since early times and now also for microwave signals.[11] Nevertheless, instead of using a dc electric field, we choose the dc bias magnetic field for both low-frequency magnetic and electric signals. An interesting advantage is the elimination of internal electrodes within the cell.

We first demonstrate the proof-of-principle operation by sensing low-frequency magnetic signals with Rydberg level $60^2S_{1/2}$, where Ω_c is about $2\pi\times 2.1$ MHz at the center of the 480 nm beam. A separate coil feeds the low-frequency magnetic signals to the system for detection.

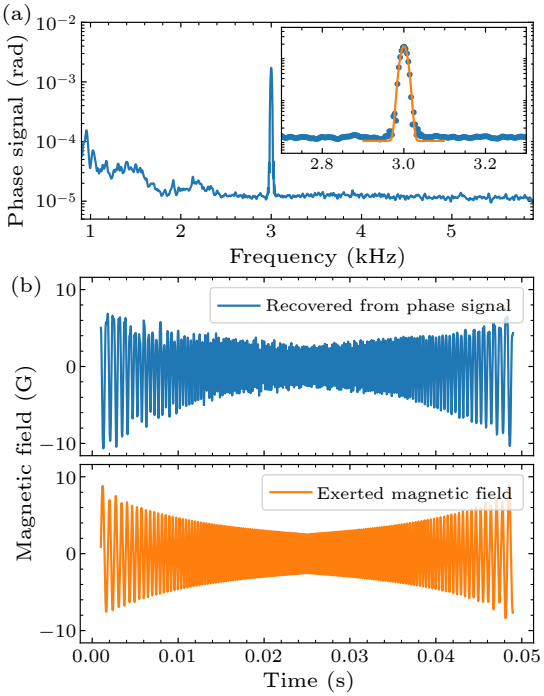

Fig. 2. Results of low-frequency magnetic field. (a) Spectrum of the demodulated EIT probe phase signal. The inset shows the Lorentz fitting. Here, the signal-to-noise ratio (SNR) is 150.5, and the estimated sensitivity at 3.0 kHz is $0.87\,\mu\mathrm{T}/\sqrt{\mathrm{Hz}}$. (b) Performance with frequency-modulated (FM) signal, comparing the recovered signal (up) and the exerted magnetic field (down). The linear-chirped signal has a center frequency of 3.0 kHz, an FM range of ±2.0 kHz, and an FM speed of 20.0 Hz. The signal undergoes a band-pass filter with a bandwidth of 700 Hz–6000 Hz. The effective sensitivity here is $3.73\,\mu\mathrm{T}/\sqrt{\mathrm{Hz}}$.

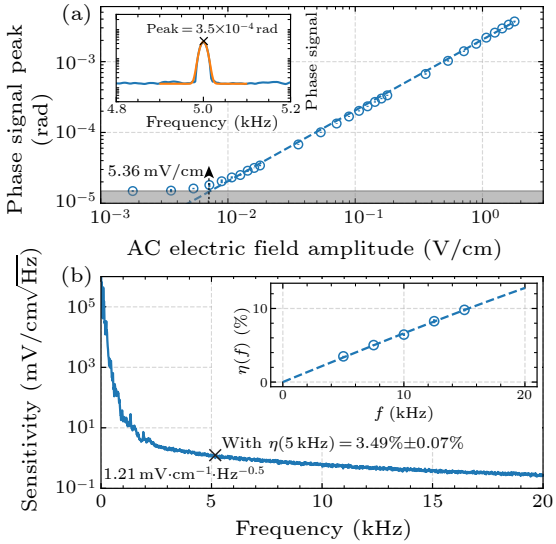

Fig. 3. Peak amplitude in the frequency spectrum of the demodulated phase signal with different electric signal amplitudes at a frequency of 5 kHz, under an 18 G bias magnetic field. This series of measurements aims to evaluate (a) the lowest detectable field and (b) sensitivity. The inset of (a) shows a typical signal spectrum, while the inset of (b) shows the measured screening ratios.

Here, the dc bias magnetic field lifts the degeneracy of the $m_J = \pm 1/2$ sublevels and puts the Zeeman shift into its linear regime for the incoming-signal-induced perturbations. Figure 2(a) shows a typical trace of data where the dc bias magnetic field is 1.9 G and the exerted sinusoidal signal has an amplitude of 8.3 G and a frequency of 3.0 kHz. To check the dynamic range, we use the same apparatus to measure a linearly chirped signal as shown in Fig. 2(b) with the recovered signal in time domain from demodulation.

Now we discuss another main topic of sensing low-frequency electric signals, which has vast opportunities in various applications. For improved sensitivity to electric fields and enhanced coupling strength with the driving laser, we choose to work with Rydberg D states as the destination of two-photon ground-Rydberg excitation. More specifically, we perform a series of experiments on the Rydberg state $58^2\mathrm{D}5/2$ under a dc bias magnetic field and summarize the results in Fig. 3, where Ω_c is about $2\pi \times 3.7$ MHz at the center of the 480 nm beam. The probe laser and the coupling laser are both vertically polarized. A set of metal field plates acts as the source of low-frequency electric signals, and the applied electric signal is fixed at 5 kHz while its amplitude is varied to evaluate the sensitivity.

Our results contain one special feature of the ambient first-order response with respect to the incoming signal frequency. Namely, a low-frequency electric field with frequency ω_l will induce a phase modulation at frequency ω_l. This may initially look surprising because a pure 58D state exhibits only a second-order Stark effect in weak fields. According to our theoretical and experimental investigations [see the Supplementary Materials (SM) for more details], this first-order response most likely stems from the Rydberg dipole–dipole interactions that extensively exist in the atomic vapor.

More specifically, we estimate that the average interatomic distance between two ^{87}Rb atoms is about 4 µm. At such distances or even closer, the Rydberg dipole–dipole interaction induces the Förster resonance between two atoms. Therefore, the destination state of the Rydberg EIT is no longer a purely 58D state but a linear superposition of D state plus nearby S, P, F states. Subsequently, the first-order Stark effect occurs, which has a linear dependence of the frequency shift on the electric field amplitude. This effect generates the first-order response in our heterodyne detection of low-frequency fields via Rydberg EIT with phase demodulation, where the first-order response is significantly stronger than the higher orders as we observe experimentally.

As a consequence of the quantum defect, some Rydberg states of lower orbital angular momentum can lift the energy degeneracy. When a small electric field interacts with a Rydberg state $|\psi\rangle$, the first-order perturbed energy $\langle\psi|\boldsymbol{E}\cdot\boldsymbol{x}|\psi\rangle$ is zero because the parity of $\boldsymbol{x}$ is odd. This indicates that $|\psi\rangle$ does not have the linear Stark effect associated with the first-order perturbation. On the other hand, when the Rydberg dipole–dipole interaction and even Förster resonance take place,[4,44] $|\psi\rangle$ becomes a linear superposition of states with different angular momenta. Then $\langle\psi|\boldsymbol{E}\cdot\boldsymbol{x}|\psi\rangle$ has a nonzero value, so that the

response follows the linear Stark effect. Additionally, photoionization by the 480 nm laser may also produce a bias electric field inside the cell,[21] thereby contributing to the observed linear Stark effect.

The screening effect against external electric fields by the metallic alkali atom layer on the vapor cell interior shows a frequency-dependent behavior,[21] as we have also observed experimentally. Due to the screening effect, the low-frequency electric field experienced by atoms inside the glass cell constitutes only a small fraction of the external field. The lowest detectable signal strength and sensitivity with respect to purely atom-field interaction need to include a quantitative analysis of the screening effect. We evaluate this via two experimental methods, including utilization of the second-order Stark effect near the Rydberg EIT transparency point and calibration between the Rydberg EIT amplitude and phase signals. The screening ratio is measured to be approximately 3.5% at 5 kHz.

We measure the peak amplitude in the frequency spectrum of the demodulated phase signal as a function of incoming electric signal amplitude, where the peak value is read out from the FFT spectrum with a total integration time of 0.1 s, as shown in Fig. 3. At this moment, the minimum detectable field amplitude is 5.36 mV/cm outside the vapor cell. By calculating the SNR of the FFT spectrum, we obtain the sensitivity of our measurement to be 1.21 $\mathrm{mV{\cdot}cm^{-1}{\cdot}Hz^{-0.5}}$. With this screening ratio value, our result represents a minimal detectable electric field of 186 μV/cm and sensitivity down to 42.4 $\mathrm{\mu V{\cdot}cm^{-1}{\cdot}Hz^{-0.5}}$ in-cell as seen by the ^{87}Rb atoms.

Here, applying the dc bias magnetic field also helps to lift the degeneracies and can technically even help to improve performance if the Zeeman-shifted states have better response to the electric field. Figure 4 shows the typical results of such measurements. In particular, we observe that even at 0 bias magnetic field, the linear response holds well and is not the cause of the first-order response.

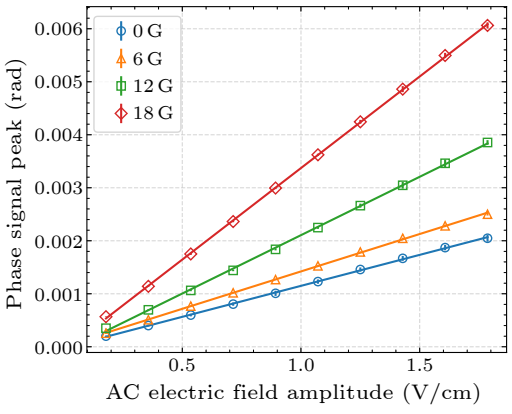

Fig. 4. Performance with respect to different amplitudes for incoming electric signals at 5.0 kHz. The dc bias magnetic field is parallel to the AC electric field. The error bars represent one standard deviation from five independent experiments, and the solid lines are linear fits. The slopes from 0 G to 18 G are $(1.17 \pm 0.01) \times 10^{-3}$, $(1.41 \pm 0.01) \times 10^{-3}$, $(2.20 \pm 0.02) \times 10^{-3}$, and $(3.45 \pm 0.01) \times 10^{-3}$ rad·cm/V, respectively.

Meanwhile, linearity holds well between the peak amplitude of demodulated phase signals and the amplitudes of exerted electric fields within the shown range. This stems from the combination of linearity in EIT response as in Eq. (2) and linearity in the first-order Stark effect as shown in Fig. 3. We have also conducted heating and cooling processes on the vapor cell and then observed that the retrieved signal strength has a positive correlation with temperature (see the SM for more details). In other words, the higher atomic density leads to an enhanced phase signal, which corroborates our previous analysis about the dipole–dipole interactions.

We further examine the frequency-dependent properties of the system and obtain the results shown in Fig. 5, which also suggests favorable characteristics in terms of frequency dynamic range and instantaneous bandwidth. Overall, we think that the main reason for the seemingly linear dependence on frequency in Fig. 5 corroborates the behavior of the screening effect, namely that the metallic layer of the vapor cell functions like a high-pass filter for incoming low-frequency electric signals.[23] The frequency range under investigation in Fig. 5 is, in fact, relatively small compared with the full range where the screening effect has significant influences. There are also other factors that can possibly contribute to frequency dependence, such as the intrinsic properties of demodulation instruments.

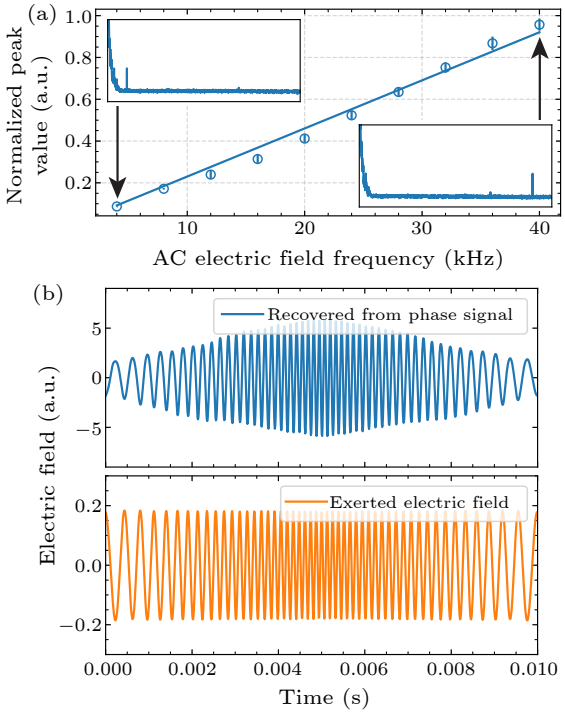

Fig. 5. Frequency-dependent responses. (a) Signals of different frequencies at a constant amplitude. The error bars represent one standard deviation from five independent experiments, and the solid line is to guide the eye. The insets show the complete spectrum of demodulated phase signals. (b) Performance with respect to FM electric signals. The linear-chirped signal has a center frequency of 5.0 kHz, an FM range of ±3.0 kHz and an FM speed of 100.0 Hz. The signal undergoes a band-pass filter with a bandwidth of 1 kHz–10 kHz.

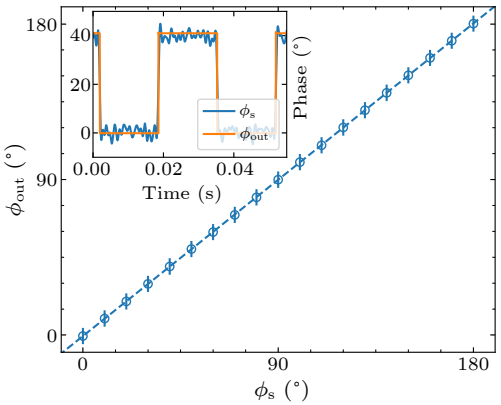

Fig. 6. Measured phase $\phi_{\rm out}$ versus the original phase $\phi_{\rm s}$ of the applied electric field. Inset: temporal response of $\phi_{\rm out}$ as the original phase switches between 0° and 20° at 30 Hz.

Figure 6 demonstrates our system's capability to characterize both the amplitude and phase of electric fields while clarifying two distinct "phases": the laser-related phase $\Phi_{\rm Rydberg}(t)$—linked to our detection method—and the target field's intrinsic phase $\phi_{\rm s}$. To extract $\phi_{\rm s}$, we apply a second digital lock-in detection: we mix $\Phi_{\rm Rydberg}(t)$—linearly linked to the intra-cell field through dispersion and the first-order Stark effect—with $\cos(\omega_{\rm s}t)$ and $\sin(\omega_{\rm s}t)$, filter high frequencies, then compute $\phi_{\rm out} = \arctan(y_{\rm out}/x_{\rm out}) = \phi_{\rm s}$. As shown, $\phi_{\rm out}$ exhibits a linear response to $\phi_{\rm s}$. The inset further confirms dynamic phase tracking, capturing $\phi_{\rm s}$ switching between 0° and 20° at 30 Hz. For a frequency-modulated field with a 5.0 kHz center frequency and a range of ±2.0 kHz, observed amplitude modulation also reveals glass cell screening—this effect attenuates lower frequencies and reduces the field's penetration into the cell.

Currently, our results remain significantly distant from the standard quantum limit.[9,45] While the screening effect constitutes the major challenge for low-frequency electric field detection, typical adverse effects associated with quantum sensing in atomic vapor, such as Doppler effects from different atomic velocity groups and inter-atomic collisions, can also influence the experiment. Furthermore, realistic atomic states and linkage patterns are significantly more complex than those in the idealized three-level atom model. Besides the screening effect, technical noise below ∼2 kHz from instruments can also pose a major constraint on further extension to lower frequencies, calling for improvements in cell material and advanced noise suppression techniques.

In conclusion, we have designed and demonstrated an effective method for quantum sensing of low-frequency fields with Rydberg atoms via phase modulation and demodulation. It applies to both the low-frequency magnetic and electric fields. Our results hint at the possibility of integrating the detection of both low-frequency magnetic and electric fields into a single compact atom-based device. The information about incoming low-frequency fields is received as phase modulation of the probe laser in the Rydberg EIT transparency window, and the scalability of our method can become another important factor in potential applications. The observed linear response to the low-frequency electric field signals is an example of how the many-body interactions help to enhance the performance of quantum sensing processes. At this moment, the measurement relies solely on the Rydberg dipole–dipole interactions of ^{87}Rb. Extending this study to two- and multi-species systems[46,47] appears promising for exploring further improvements and additional functionalities.

Acknowledgements. This work was supported by the Science and Technology Commission of Shanghai Municipality (Grant No. 24DP2600202), the National Key R&D Program of China (Grant No. 2024YFB4504002), Industrial Technology Development Research Program of Shanghai Institute of Optics and Fine Mechanics, the National Natural Science Foundation of China (Grant No. 92165107), and the China Postdoctoral Science Foundation (Grant Nos. 2024M753359 for S. J. and 2022M723270 for X.W.).

References

[1] Degen C L, Reinhard F, and Cappellaro P 2017 *Rev. Mod. Phys.* **89** 035002
[2] Schlossberger N, Prajapati N, Berweger S, Rotunno A P, Artusio-Glimpse A B, Simons M T, Sheikh A A, Norrgard E B, Eckel S P, and Holloway C L 2024 *Nat. Rev. Phys.* **6** 606
[3] Zhang H, Ma Y, Liao K, Yang W, Liu Z, Ding D, Yan H, Li W, and Zhang L 2024 *Sci. Bull.* **69** 1515
[4] Saffman M, Walker T G, and Mølmer K 2010 *Rev. Mod. Phys.* **82** 2313
[5] Sedlacek J A, Schwettmann A, Kübler H, Löw R, Pfau T, and Shaffer J P 2012 *Nat. Phys.* **8** 819
[6] Sedlacek J A, Schwettmann A, Kübler H, and Shaffer J P 2013 *Phys. Rev. Lett.* **111** 063001
[7] Anderson D A, Miller S A, Raithel G, Gordon J A, Butler M L, and Holloway C L 2016 *Phys. Rev. Appl.* **5** 034003
[8] Han J, Vogt T, Gross C, Jaksch D, Kiffner M, and Li W 2018 *Phys. Rev. Lett.* **120** 093201
[9] Cox K C, Meyer D H, Fatemi F K, and Kunz P D 2018 *Phys. Rev. Lett.* **121** 110502
[10] Jing M, Hu Y, Ma J, Zhang H, Zhang L, Xiao L, and Jia S 2020 *Nat. Phys.* **16** 911
[11] Ouyang K, Shi Y, Lei M, and Shi M 2023 *Appl. Phys. Lett.* **123** 264001
[12] Liu Z K, Zhang L H, Liu B, Zhang Z Y, Guo G C, Ding D S, and Shi B S 2022 *Nat. Commun.* **13** 1997
[13] Tu H T, Liao K Y, Wang H L, Zhu Y F, Qiu S Y, Jiang H, Huang W, Bian W, Yan H, and Zhu S L 2024 *Sci. Adv.* **10** eads0683
[14] Downes L A, Torralbo-Campo L, and Weatherill K J 2023 *New J. Phys.* **25** 035002
[15] Cai Y, Shi S, Zhou Y, Li Y, Yu J, Li W, and Li L 2023 *Phys. Rev. Appl.* **19** 044079
[16] Elgee P K, Hill J C, LeBlanc K J E, Ko G D, Kunz P D, Meyer D H, and Cox K C 2023 *Appl. Phys. Lett.* **123** 084001
[17] Calero V, Fernández-Mateo R, Morgan H, García- Sánchez P, and Ramos A 2021 *Phys. Rev. Appl.* **15** 014047
[18] Meyer D H, Kunz P D, and Cox K C 2021 *Phys. Rev. Appl.* **15** 014053
[19] Ding Z, Liu Y, Yang K, Li Y, Ran R, Lin Y, and Fu Y 2024 *IEEE Trans. Antennas Propag.* **72** 9558
[20] Ding Z, Liu Y, Yang K, Li Y, Ran R, Lin Y, and Fu Y 2025 *IEEE Antennas Wireless Propag. Lett.* **24** 247
[21] Jau Y Y and Carter T 2020 *Phys. Rev. Appl.* **13** 054034

[22] Mohapatra A K, Bason M G, Butscher B, Weatherill K J, and Adams C S 2008 *Nat. Phys.* **4** 890

[23] Lim M J, Cervantes M, Brady C, McPoyle S, and Simmermon J 2023 *Appl. Phys. Lett.* **123** 051106

[24] Li L, Jiao Y, Hu J, Li H, Shi M, Zhao J, and Jia S 2023 *Opt. Express* **31** 29228

[25] Lei M and Shi M 2024 *Opt. Lett.* **49** 5547

[26] Savukov I M, Seltzer S J, Romalis M V, and Sauer K L 2005 *Phys. Rev. Lett.* **95** 063004

[27] Chalupczak W, Godun R M, and Pustelny S 2018 *Adv. Atomic Mol. Opt. Phys.* **67** 297

[28] Budker D and Romalis M 2007 *Nat. Phys.* **3** 227

[29] Allred J C, Lyman R N, Kornack T W, and Romalis M V 2002 *Phys. Rev. Lett.* **89** 130801

[30] Zhao B, Li L, Zhang Y, Tang J, Liu Y, and Zhai Y 2023 *IEEE Sens. J.* **23** 18949

[31] Deans C, Cohen Y, Yao H, Maddox B, Vigilante A, and Renzoni F 2021 *Appl. Phys. Lett.* **119** 014001

[32] Maddox B and Renzoni F 2023 *Appl. Phys. Lett.* **122** 144001

[33] Kominis I K, Kornack T W, Allred J C, and Romalis M V 2003 *Nature* **422** 596

[34] Dang H B, Maloof A C, and Romalis M V 2010 *Appl. Phys. Lett.* **97** 151110

[35] Budker D, Kimball D F, Rochester S M, Yashchuk V V, and Zolotorev M 2000 *Phys. Rev. A* **62** 043403

[36] Fleischhauer M, Imamoglu A, and Marangos J P 2005 *Rev. Mod. Phys.* **77** 633

[37] Qu W, Jin S, Sun J, Jiang L, Wen J, and Xiao Y 2020 *Nat. Commun.* **11** 1752

[38] Zhang X, Jin S, Qu W, and Xiao Y 2021 *Appl. Phys. Lett.* **119** 054001

[39] Hammerer K, Sørensen A S, and Polzik E S 2010 *Rev. Mod. Phys.* **82** 1041

[40] Finkelstein R, Bali S, Firstenberg O, and Novikova I 2023 *New J. Phys.* **25** 035001

[41] Yang W, Jing M, Zhang H, Zhang L, Xiao L, and Jia S 2023 *Phys. Rev. Appl.* **19** 064021

[42] Osterwalder A and Merkt F 1999 *Phys. Rev. Lett.* **82** 1831

[43] Lu X, Sun Y, and Metcalf H 2011 *Phys. Rev. A* **84** 033402

[44] Saffman M 2016 *J. Phys. B: At. Mol. Opt. Phys.* **49** 202001

[45] Tu H T, Liao K Y, Wang H L, Zhu Y F, Qiu S Y, Jiang H, Huang W, Bian W, Yan H, and Zhu S L 2024 *Sci. Adv.* **10** eads0683

[46] Zeng Y, Xu P, He X, Liu Y, Liu M, Wang J, Papoular D J, Shlyapnikov G V, and Zhan M 2017 *Phys. Rev. Lett.* **119** 160502

[47] Sun Y 2024 *Sci. China Phys. Mech. Astron.* **67** 120311